International Journal of
INTELLIGENT SYSTEMS AND APPLICATIONS IN ENGINEERING
ISSN:2147-6799 www.ijisae.org Original Research Paper

Performance Evaluation of Maximal Overlap Discrete Wavelet Transform Families with Bidirectional Long Short-Term Memory for High Impedance Fault Detection

Rini Varghese P[1,3], M.S.P. Subathra[2*]

Submitted: 14/05/2024 **Revised**: 27/06/2024 **Accepted**: 07/07/2024

Abstract: Maximal Overlap Discrete Wavelet Transform (MODWT) is employed to characterize three-phase current signals for high impedance fault (HIF) detection. However, a few vital issues, like the classification of HIF from non-HIF, have not yet been benefited by MODWT families and Bi-LSTM. Hence, in this paper, the performance of four families of MODWT, namely, Coiflets (coif), Daubechies (db), Fejer-Korovkin (fk), and Symlets (sym) were studied. A radial distribution network was simulated, and three-phase currents were taken during HIF and non-HIF conditions. Further, this paper attempts to identify the best of the four MODWT families and the level of decomposition required to analyze the current signals. The nine statistical features are extracted from the wavelet coefficients, Kruskal Wallis test is carried out to select the best features and fed into the Bi-directional LSTM(Bi-LSTM) classifier. From the results, it was found out that the coif attained the highest classification accuracy for all the levels of decomposition.

Keywords: *High Impedance fault, Maximal Overlap Discrete Wavelet Transform, Bi-directional LSTM, Fault detection.*

1. Introduction

Distribution networks are highly vulnerable to interruptions in power quality, primarily resulting from three types of operational failures: HIF, voltage disturbances, and short-circuit faults. HIF stands out as one of the most concerning in this context, primarily because the fault current is typically below the threshold for overcurrent devices like relays, reclosers, and fuses, meaning that it is not usually eliminated by the traditional protection system. Furthermore, HIF poses a risk to the public due to the potential for electric shock as well as the potential for fire because of arcing.

A high-impedance surface (HIF) is created when an electrically charged conductor makes contact with something like sand, asphalt, or even tree branches[1]. If all the disturbances are examined in the time domain, it may be confused for other disturbances like feeder and load energizing or capacitor bank switching. On the other hand, HIF exhibits unique properties in the frequency domain that make them detectable. Multi-resolution transforms are more appropriate for analyzing HIF signals because they are not stationary.

[1]*Department of Electrical and Electronics Engineering, School of Engineering and Technology, Karunya Institute of Technology and Sciences, Coimbatore-641114, Tamil Nadu, India.*
[2]*Department of Robotics Engineering, School of Engineering and Technology, Karunya Institute of Technology and Sciences, Coimbatore-641114, Tamil Nadu, India.*
[3]*Department of Electrical and Electronics Engineering, Mar Baselios Institute of Technology and Science, Nellimattom 686693, India*
**Corresponding authors: Dr. M.S.P. Subathra (subathra@karunya.edu)*

The proposed work uses three-phase current signals from a radial distribution system. The nine statistical features are extracted using MODWT families, the Kruskal wallis test is used to select the best features, and then the HIF /Non-HIF classification is done using Bi-LSTM.

1.1. Literature review

In [2],a novel approach to identifying power quality (PQ) disturbances, focusing on voltage sags and interruptions associated with diverse faults such as transmission line, feeder, and transformer faults, is introduced. The method employs a MODWT-based PQ detection algorithm that accurately pinpoints the initiation and recovery of disturbances. The algorithm showcases strong performance even without a detection threshold and isn't reliant on the sampling frequency of PQ data. To combat noise, it transforms pre-processed PQ waveforms into 2D binary vectors via space vector transformation. Subsequently, a resilient classifier is proposed, employing an enhanced stacked sparse denoising autoencoder coupled with supervised backpropagation training. The technique maintains high detection accuracy, even when faced with limited training samples detecting various PQ disturbances[17].

The[3] paper introduces a time-series-based method utilizing maximal overlap discrete wavelet transform (MODWT) for detecting and locating diverse power quality (PQ) disturbances. Ten different PQ events in voltage signals, such as sag, swell, interruption, harmonic, spike, notch, etc., are investigated using this wavelet transform. Signal decomposition up to the fourth level

with MODWT provides coefficients for feature extraction, which act as inputs for classifiers like Support Vector Machine (SVM) and Decision Tree (DT). In the detection phase, signals are decomposed up to four levels of refinement, while in the classification phase, signals undergo similar decomposition. Comparative analysis reveals that DT outperforms SVM in classification accuracy across various scenarios, including those with and without noise. Furthermore, DT shows satisfactory performance with both synthesized and real signals, presenting a quicker and more straightforward alternative to SVM.

As in [4], a practical 400-kV Dual Circuit Transmission Line within the Indian network features a newly introduced fault diagnosis framework for the identification and categorization of cross-country side Faults (CCF) with HIF syndrome. This innovative approach comprises a three-step procedure involving signal preprocessing, detection of high impedance faults (HIFs), and subsequent classification using specific fault classifier protocols. These protocols are precisely determined based on fault coordinates within a normalized 3D Fault Plane. The effectiveness of this method has been successfully demonstrated across various operational and switching scenarios, including capacitor bank switching, reactor string switching, and load/feeder switching. Extensive testing has been conducted to evaluate the resilience of the diagnostic scheme against noise, nonlinear loads, and light-load conditions[18]. Comparative analyses have been performed for both common cause faults (CCF) and CCF-HIFs. Notably, the proposed scheme demonstrates an operational time within five cycles from when a HIF is detected.

Electroencephalogram (EEG) signal analysis has extensively used wavelet transforms for automated diagnosis of epileptic seizures[5]. Four cases—normal-generalized epilepsy (i), normal-focal epilepsy (ii), normal-focal-generalized (iii), and normal-epilepsy (iv)—are used to assess the suggested methodology. The study also attempts to define the necessary degree of decomposition for EEG signal analysis and identify the best wavelet function among seven popular wavelet families. The wavelet coefficients are used to extract nine statistical features, which are then fed into the support vector machine (SVM) classifier. The results of the experiments show that, out of all the experimental cases, Discrete Wavelet Transform (DWT) with rbio1.1 achieves the best classification accuracy.

2. Methodology adopted

Step 1: Model the system to be studied – In the study, the radial topology of the distribution feeder is modeled MATLAB and faults like HIF, Non-HIF ((Line to ground (LG), Line to Line (LL), Line to line to ground(LLG) and line to line to line to ground(LLLG)) were created.

Step 2: Data acquisition – By varying the fault resistances and ground resistances, different cases of Non-HIF and HIF were obtained.

Step 3: Feature Extraction-Four MODWT families (coif, db, fk, sym) each were applied to extract the features of the faults and statistical features were taken.

Step 4: Feature Selection- Kruskal Wallis test is done to get the best features that can contribute to the classifier for better accuracy.

Step 5: Classifier – Selected features are input to the Bi-LSTM classifier for discriminating HIF and non-HIF events.

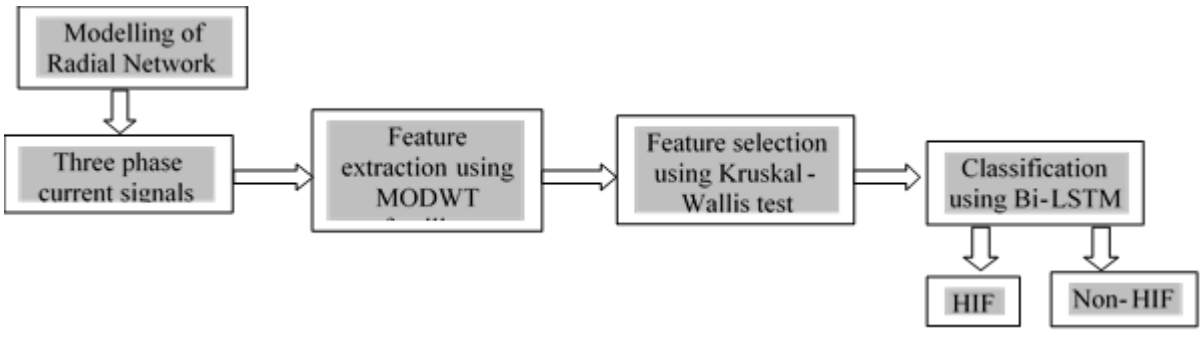

Fig 1 Flow diagram showing various steps involved.

2.1 Radial distribution network

Radial distribution networks are often used to service areas with medium and light loads from a single source, with good voltage regulation and reliability and reduced cable congestion [1]. The drawback of using the radial system is if any of the feeders becomes faulty, the entire system experiences blackouts that might lead to expensive repairs and productivity loss [6], [7]. A power distribution network is modeled using a sim-power system block. The HIF and Non-HIF conditions are created in the model, and fault current waveforms are taken for analysis [8]. The

model consists of a grid source 50MVA/138kV, a transformer 50MVA, and 138kV/25kV with an integrated load facility. The power grid frequency is 50 Hz, and the distribution line length is 100 km. The single-line diagram of the radial distribution system with the HIF model is shown in Fig 2.

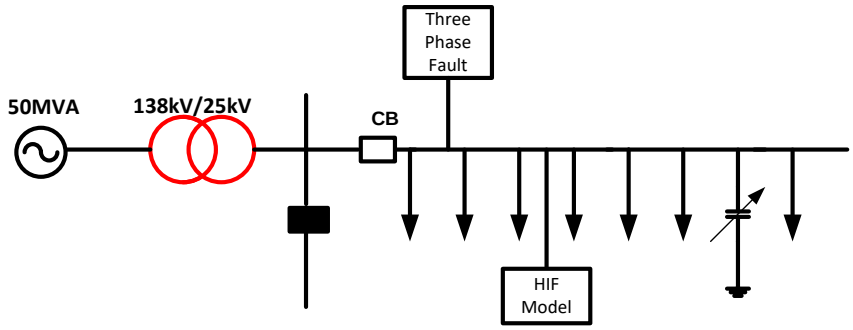

Fig 2 Single line diagram of radial distribution network.

The waveforms shown in Fig.3(a) show the time-varying current waveforms during normal conditions in which the normal three-phase current rating is 175A and the three-phase voltage 20kV. A total of 1000 cases of faults, including HIF, LGF, LLF, LLGF, and LLLGF, were taken for the input to feature extraction techniques[9].

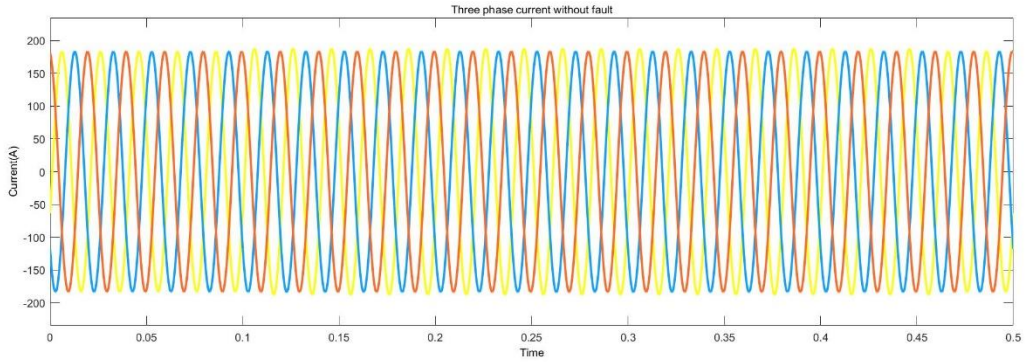

(a)

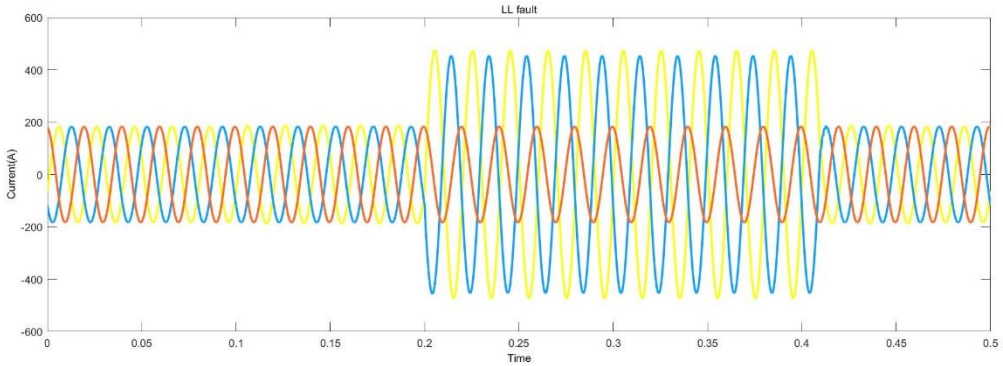

(b)

Fig.3 (a) Current waveform at normal conditions,. **(b)** Faulty condition: current waveform of LL fault in RB phase

HIF is a set of power system disturbances that occur in an MV distribution system(15kV to 25 kV), which produces a low-range fault current(<100A) difficult for conventional relays to detect [10]. The fault occurs when a charged conductor touches the high grounding impedance surfaces such as trees, sand, cement, wet soil, etc., or can be due to a broken or unbroken conductor that possesses dynamic features like asymmetry, randomness, non-linearity, shoulder, build-up and intermittence [9]. Modelling HIF is important to exhibit the features of HIF characteristics. Many models [11], such as the Emanual arc model [12], Mayr's model[13], kizilcay model[14], and Matthews's arc model[10] can be used to model HIF, of which the Emanual arc model is used for this study.

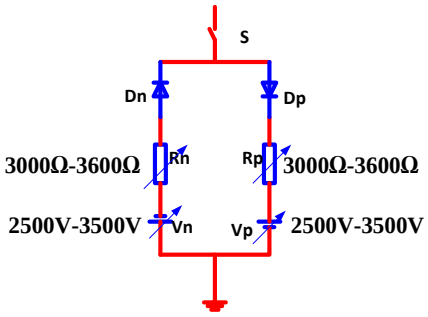

Fig.4 Emmanuel arc model of HIF

Fig.4 shows the modeling of HIF using the Emmanuel arc model [15], having two anti-parallel diodes (Dn, Dp), voltage sources(Vn, Vp), and nonlinear resistors (Rn, Rp). The diodes mimic the randomness during positive and negative half cycles. The voltage source represents the arcing voltage between the distribution lines, trees, soil or air that produces asymmetry during positive and negative half cycles, and the resistors represent the resistance offered by the trees or earth resistance.

The waveform shown in 5(a)&5(b) represents the fault voltage and current during HIF inception at 0.1s to 0.45s. A total of 1000 HIF cases were taken, creating HIF in Phases A, B, and C. The voltage range is 25kV, and the current ranges from 5-20A depending on the fault resistances varied from 3000Ω-3600Ω.

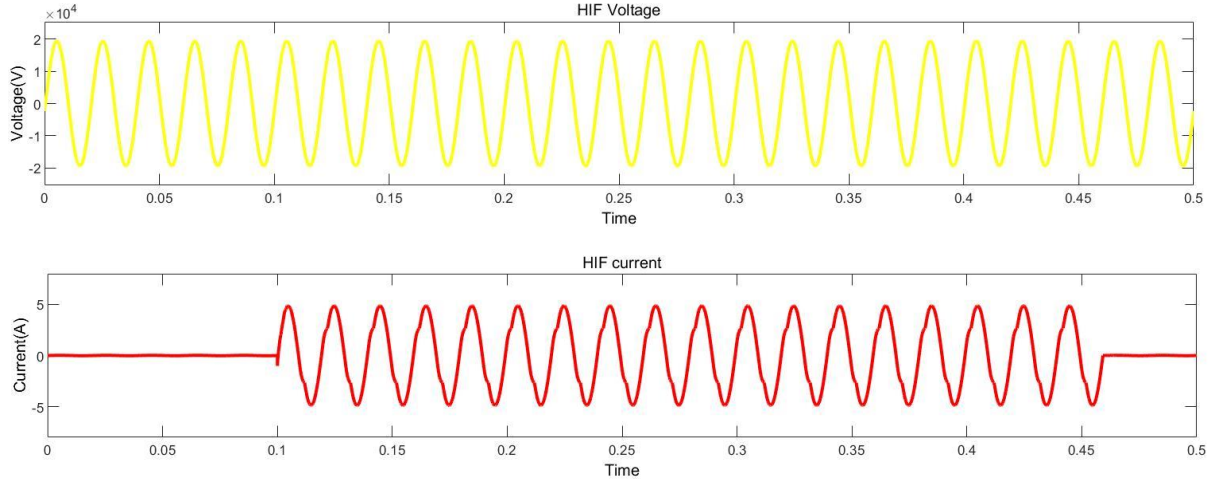

Fig 5(a) & 5(b) HIF current and voltage waveform

2.2 Maximal Overlap Discrete Wavelet Transform

The improved version of the DWT that allows for the free selection of the beginning point time series signal [1] and also a non-orthogonal variation of the traditional DWT is MODWT [16]. The DWT filter can be equated to the wavelet filter $\tilde{g}_l$ and the MODWT scaling filter $\tilde{h}_l$ via (1) and (2).

$$\tilde{h}_l = \frac{h_l}{\sqrt{2}} \quad (1)$$

$$\tilde{g}_l = \frac{g_l}{\sqrt{2}} \quad (2)$$

Also, the MODWT filters are given by the equation (3) and (4)

$$\tilde{g}_l = (-1)^{l+1} h_{L-1-l} \quad (3)$$

$$\tilde{h}_l = (-1)^{l+1} g_{L-1-l} \quad (4)$$

where L is the filter width and l = 0, 1, 2,..., L − 1. Along with the MODWT scaling coefficients and the input time series signal Y (n), the nth element of the first-stage wavelet.

$$\widetilde{W}_{1,n} = \sum_{l=0}^{L_1-1} \tilde{h}_l X_{n-l} \ \ mod\ N \quad (5)$$

$$\tilde{V}_{1,n} = \sum_{l=0}^{L_1-1} \tilde{g}_l X_{n-l} \ \ mod\ N \quad (6)$$

Where n= 1, 2, 3,..., N(length of signal in sample)

$$\tilde{A}_{1,n} = \sum_{l=0}^{L_1-1} \tilde{g}_l \tilde{V}_{1,n+l} \ \ mod\ N \quad (7)$$

$$\widetilde{D}_{1,n} = \sum_{l=0}^{L_1-1} \tilde{g}_l \widetilde{W}_{1,n+l} \ \ mod\ N \quad (8)$$

The first-stage approximations and details can be calculated by (7) and (8). The MODWT scaling coefficients $\tilde{V}_j$ and $\widetilde{W}_j$ wavelet coefficients at the n[th] element of the j[th] stage are given by the eqns. (9) and (10). Fig 4 represents the block diagram of MODWT decomposition.

$$\tilde{V}_{j,n} = \sum_{l=0}^{L_j-1} \tilde{g}_{j,1} \tilde{X}_{n-l} \ \ mod\ N \quad (9)$$

$$\widetilde{W}_{j,n} = \sum_{l=0}^{L_j-1} \tilde{h}_{j,1}\tilde{X}_{n-l} \ \ mod\ N \qquad (10)$$

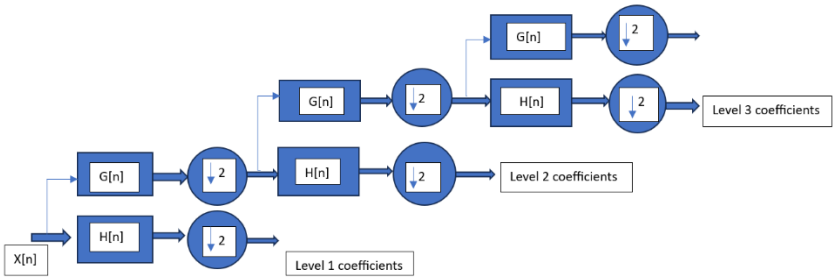

Fig 6 Block diagram representation of MODWT decomposition.

The approximations $\tilde{A}_j$ and the details $\tilde{D}_j$ of the nth element of the jth stage MODWT are given by the (11) and (12).

$$\tilde{A}_{j,n} = \sum_{l=0}^{L_j-1} \tilde{g}_{j,l}^{0}\tilde{V}_{1,n+l} \ \ mod\ N \qquad (11)$$

$$\tilde{D}_{j,n} = \sum_{l=0}^{L_j-1} \tilde{h}_{j,l}^{0}\widetilde{W}_{1,n+l} \ \ mod\ N \qquad (12)$$

Using MODWT, the nine statistical features are extracted, and the details are shown in Table 1. After feature extraction, the Kruskal wallis test is run to get the best results, which makes the classification easy for the classifier. Table 2 shows the comparison of various MODWT families.

Table 1. Statistical features extracted using MODWT.

Features	Equations
Min	$\min(C_i)$
Max	$\max(C_i)$
Mean	$\mu_i = \frac{1}{N}\sum_{i=1}^{N} c_i$
STD	$\sigma_i = \sqrt{\frac{1}{N}\sum_{i=1}^{N}(c_i - \mu_i)^2}$
Kurthosis	$k_i = \frac{(1/N)\sum_{i=1}^{N}(c(i) - \mu_i)^4}{N\sigma^4}$
Skewness	$s_i = \frac{(1/N)\sum_{i=1}^{N}(c(i) - \mu_i)^3}{N\sigma^3}$
Energy	$e_i = \frac{1}{N}\sum_{i=1}^{N}\lvert c_i\rvert^2$
nSTD (Ratio between STD and difference of min max values)	$n\sigma_i = \frac{\sigma_i}{max_i - min_i}$
nEnergy (Ratio between energy and size of the band)	$ne_i = \frac{e_i}{length\ (c_i)}$

Table 2 Comparison of MODWT families

Sl.No	Family	Short name	Order	Support width	Filter length
1	Coiflets	coif	N = 1, 2, ..., 5	1	2

2	Daubechies	db or haar	N = 1, 2, ...,45	2N-1	2N
3	Fejer-Korovkin	fk	N = 4,6,8,14,18,22	2N-1	2N
4	Symlets	sym	N = 2, 3, ... 45	6N-1	6N

2.3. Bi-directional Long short-term memory (Bi-LSTM)

Bi-LSTM is the name given to a sequence model that consists of two LSTM layers, one for processing input forward and the other for processing backward. The idea behind this strategy is that the model can better comprehend the relationship between sequences by processing data in both directions.

Two unidirectional LSTMs that process the forward and backward sequence make up the bidirectional LSTM architecture. This architecture can be understood as having two independent LSTM networks, one of which receives the token sequence in its original order and the other in reverse. The combined probability of the two outputs from the two networks is the final output, which is a probability vector.

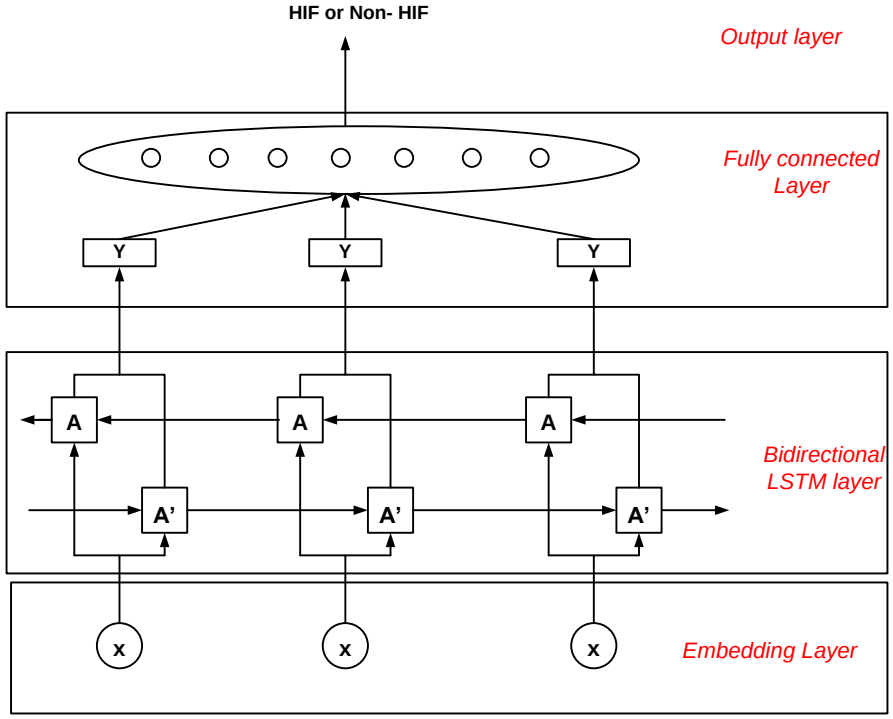

Fig.7 Bi-LSTM Architecture

With a learning rate of 0.001, the optimizer used to update the model weights is the Adaptive Moment Estimation (Adam) algorithm. For binary classification, the binary cross-entropy loss functions are employed. The model begins by employing an embedding layer to map inputs to their representations, as seen in Fig. 10. After that, it feeds the embeddings in two processing directions to the LSTM layers: the first moves forward, and the second moves in the opposite direction. The model architecture involves fully connected layers receiving LSTM outputs, with ReLU as the activation function. These fully connected layers learn and assemble data from LSTM layers to form the final output for classification. To prevent overfitting, a dropout probability of 0.2 is applied. Model performance is validated using a stratified K-fold cross-validation method with K set to 10. The sample percentage for every class is guaranteed to be identical to the stratified K-fold in every fold. The dataset is divided into K groups after it has been shuffled. Next, using K-1 (10-1) folds to fit the model, validate it using the K^{th} folds that are left (9 folds). This procedure is repeated until the final K-fold. It continues in this manner until each K-fold functions as a test set.

$$\overrightarrow{A'_t} = \overrightarrow{LSTM}(A_{t-1}, w_t, Y_{t-1}) \quad (13)$$

$$\overleftarrow{A_t} = \overleftarrow{LSTM}(A_{t+1}, w_t, Y_{t+1}) \quad (14)$$

$$A_t = [\overrightarrow{A'_t}, \overleftarrow{A_t}] \quad (15)$$

The Input data is represented by X_t, the hidden state is represented by A_t, , W_t represents the equivalent weight matrix and the output state of the Bi-LSTM structure is represented by Y_t.

3. Results and discussion

Various MODWT families are run with different levels of decomposition, and the best accuracy obtained for each case is shown in Table 3. The number of features extracted using MODWT families and the number of features selected using Kruskal Wallis tests are shown, with the time taken by the classifier for classification. From the Table, db and coif give the best results at lower levels of decomposition, and fk and sym give satisfactory results as compared with db and coif. Fig 8 shows some of the random results of all the MODWT families.

Table 3 comparison of Performance of various MODWT families with Bi-LSTM

MODWT Family	Level of decomposition	Accuracy	No of features extracted	No of features selected	Time elapsed
db1	Level4	94.59	125	75	22s
db2	Level8	100	125	135	27s
db3	Level4	100	125	75	11s
db4	level 7	97.3	125	120	23s
db5	level 1	100	125	30	6s
db6	level 3	100	125	60	12s
db7	level 4	97.3	125	75	18s
db8	level 1	100	125	30	8s
db9	level 5	100	125	90	10s
db10	level 1	100	125	30	8s
db11	level 6	94.59	125	105	22s
db12	level5	100	125	90	19s
db13	level3	97.3	125	60	15s
db14	level3	100	125	60	8s
db15	level2	100	125	45	6s
db16	level1	100	125	30	5s
db17	level3	100	125	60	17s
db18	level2	100	125	45	13s
db19	level1	97.3	125	30	6s
db20	level3	100	125	60	10s
db21	level5	100	125	90	19s
db22	level1	100	125	30	12s
db23	level1	94.59	125	30	15s
db24	level5	100	125	90	11s
db25	level1	100	125	30	5s
db26	level2	100	125	45	7s
db27	level3	100	125	60	7s
db28	level 4	100	125	75	9s

db29	level7	97.3	125	120	10s
db30	level2	100	125	45	13s
db31	level1	100	125	30	11s
db32	level1	100	125	30	12s
db34	level4	97.3	125	75	16s
db35	level2	100	125	45	8s
db36	level1	100	125	30	6s
db37	level1	100	125	30	5s
db38	level2	100	125	45	6s
db39	level6	94.59	125	105	10s
db40	level4	100	125	75	23s
db41	level3	100	125	60	16s
db42	level4	97.3	125	75	10s
db43	level1	94.59	125	30	7s
db44	level1	100	125	30	7s
db45	level2	100	125	30	6s
coif1	level1	100	125	30	5s
coif2	level1	100	125	30	16s
coif3	level 1	100	125	30	6s
coif 4	level 3	100	125	40	8s
coif 5	level 1	100	125	39	5s
fk2	level 2	100	125	45	15s
fk4	level 4	94.59	125	44	15s
fk6	level 4	100	125	75	9s
fk8	level 1	94.59	125	30	6s
fk14	level 3	94.59	125	60	20s
fk18	level 8	89.19	125	35	24s
fk22	level 6	97.3	125	105	24s
sym2	level 4	100	125	75	8s
sym3	level 4	100	125	75	17s
sym4	level 3	100	125	60	19s
sym5	level 4	100	125	75	8s
sym6	level 3	100	125	60	7s
sym7	level 1	94.59	125	90	19s
sym8	level 5	100	125	55	22s
sym9	level 6	100	125	105	20s
sym10	level 3	100	125	60	7s
sym12	level 4	97.3	125	75	10s

sym13	level 1	100	125	30	5s
sym14	level 1	100	125	30	12s
sym15	level 6	97.3	125	105	20s
sym16	level 3	100	125	60	12s
sym17	level 1	100	125	30	12s
sym18	level 1	97.3	125	90	9s
sym19	level 3	100	125	60	8s
sym20	level 1	100	125	30	6s
sym21	level 4	100	125	75	17s
sym22	level 2	100	125	45	13s
sym23	level 4	100	125	75	10s
sym24	level 1	91.89	125	30	7s
sym25	level 3	100	125	60	19s
sym26	level 2	100	125	45	7s
sym27	level 4	100	125	75	9s
sym28	level 2	100	125	45	8s
sym29	level 4	97.3	125	60	7s
sym30	level 2	94.59	125	45	12s
sym31	level 5	75.68	125	90	21s
sym33	level 2	100	125	45	24s
sym34	level 1	94.59	125	30	11s
sym35	level 1	67.57	125	30	7s
sym36	level 1	94.59	125	40	19s
sym37	level 1	100	125	30	17s
sym38	level 1	86.49	125	30	6s
sym39	level 1	67.57	125	30	19s
sym40	level 1	97.3	125	30	25s
sym41	level 1	100	125	30	7s

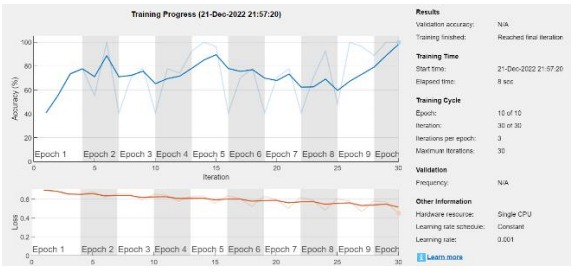

Db3 level 4

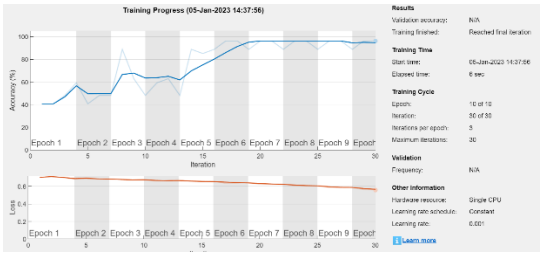

Coif 1 level 1

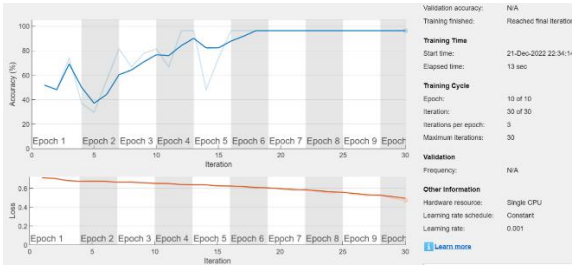

Sym 2 level 2

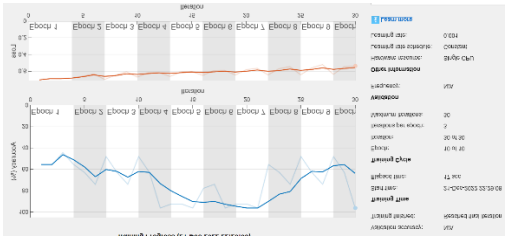

Sym 8 level 8

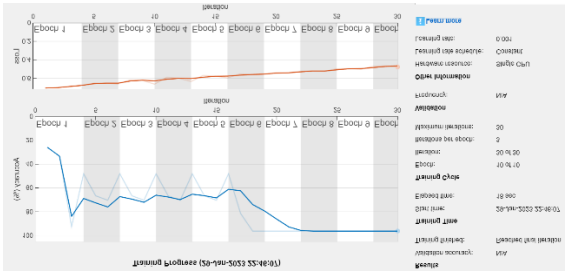

Db3 level 1

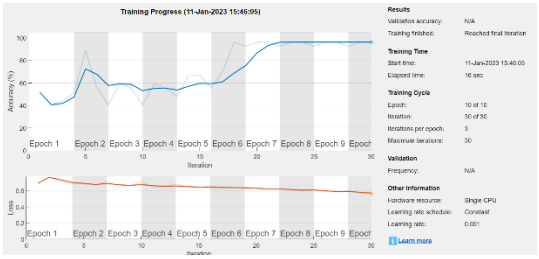

Coif 2 level 3

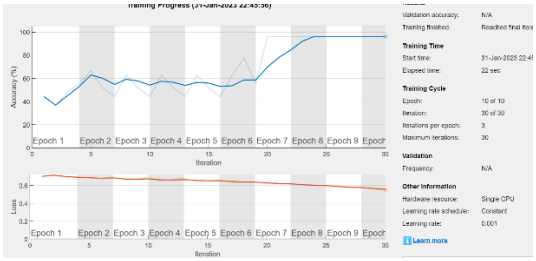

Coif 3 level 1

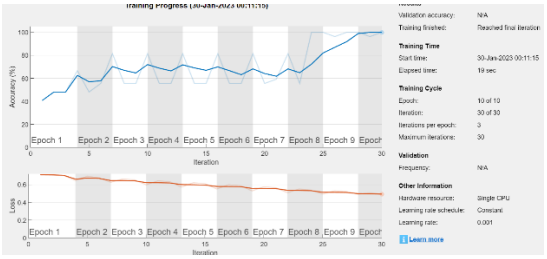

Db3 level 5

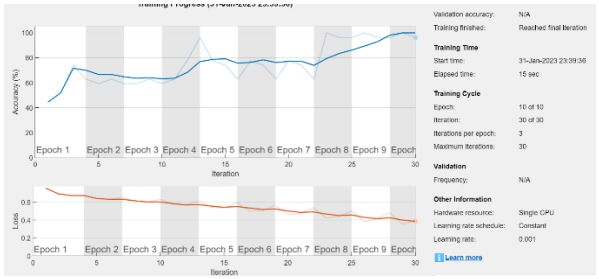

Fk4 level 4

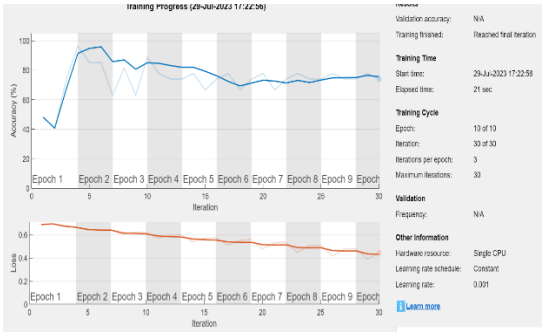

Fk22 level 6

Fig 8 Performance of various MODWT families with Bi-LSTM

4. Conclusion

To classify HIF and Non-HIF, the best possible combination of three factors—the level of decomposition, the mother wavelet, and the wavelet coefficient features—is studied in this work. The Bi-LSTM classifier obtains nine extracted statistical features. The approach is most suited for HIF detection analysis, according to the number of feature vectors and classification accuracy. The mother wavelet coif is determined to be the best wavelet family for classifying HIF based on classification accuracy. Additionally, selecting the right mother wavelet improves the performance of current signal analysis when compared to a random choice on the mother wavelet.

Availability of data and materials

The datasets used and/or analyzed during the current study are available from the corresponding author upon reasonable request.

Competing Interests

The authors have no competing interests to declare that are relevant to the content of this article.

Funding

The authors did not receive support from any organization for the submitted work.

Authors' contributions

RVP carried out the simulation, wrote the manuscript with support from MSPS. MSPS helped , conceived the original idea,supervise the project. All authors read and approved the final manuscript.

Acknowledgements

Not applicable

References

[1] Varghese P, R., Subathra, M. S. P., George, S. T., Kumar, N. M., Suviseshamuthu, E. S., & Deb, S. (2023). Application of signal processing techniques and intelligent classifiers for high-impedance fault detection in ensuring the reliable operation of power distribution systems. Frontiers in Energy Research, 11. https://doi.org/10.3389/fenrg.2023.1114230

[2] Kwon, W. H., Lee, G. W., Park, Y., Yoon, M., and Yoo, M. (1991). High impedance fault detection utilizing incremental varianc. IEEE Power Eng. Rev. 11 (4), 58–59. doi:10.1109/MPER.1991.88839

[3] Upadhyaya, S., & Mohanty, S. (2016). Localization and classification of power quality disturbances using maximal overlap discrete wavelet transform and data mining based classifiers∗. IFAC-PapersOnLine, 49(1), 437–442. https://doi.org/10.1016/j.ifacol.2016.03.093

[4] Ashok, V., & Yadav, A. (2021). Fault diagnosis scheme for cross-country faults in dual-circuit line with emphasis on high-impedance fault syndrome. IEEE Systems Journal, 15(2), 2087–2097. https://doi.org/10.1109/JSYST.2020.2991770

[5] Sairamya N.J., Premkumar M.J., George S.T., Subathra M.S.P., Performance evaluation of discrete wavelet transform, and wavelet packet decomposition for automated focal and generalized epileptic seizure detection, IETE Journal of Research, vol. 67, no. 6, pp. 778–798 (2021), DOI: 10.1080/03772063.2019.1568206

[6] Chen, J. C., Phung, B. T., Zhang, D. M., Blackburn, T., and Ambikairajah, E. (2013). Study on high impedance fault arcing current characteristics. Australas. Univ. Power Eng. Conf. AUPEC 2013. doi:10.1109/aupec.2013.6725439

[7] Zubaidi, S. L., Hashim, K., Ethaib, S., Al-Bdairi, N. S. S., Al-Bugharbee, H., & Gharghan, S. K. (2022). A novel methodology to predict monthly municipal water demand based on weather variables scenario. Journal of King Saud University - Engineering Sciences, 34(3), 163–169. https://doi.org/10.1016/j.jksues.2020.09.011

[8] P. R. Varghese, M. S. P. Subathra, C. Mathew, and S. T. George, AIP Conf. Proc. **2670**, 60004 (2022).

[9] P. R. Varghese, M. S. P. Subathra, C. Mathew, S. T. George, and N. J. Sairamya, in *Lect. Notes Electr. Eng.*, edited by P. Siano, S. Williamson, and S. Beevi (Springer Nature Singapore, Singapore, 2023), pp. 163–181.

[10] Ghaderi, A., Ginn, H. L., & Mohammadpour, H. A. (2017). High impedance fault detection: A review. Electric Power Systems Research, 143, 376–388. https://doi.org/10.1016/j.epsr.2016.10.021

[11] Elkalashy, N. I. (n.d.). Modeling and detection of high impedance arcing fault in medium voltage networks [Text.Thesis.Doctoral]. Retrieved September 20, 2024, from http://lib.tkk.fi/Diss/2007/isbn9789512290154/

[12] Sekar, K., & Mohanty, N. K. (2020). A fuzzy rule base approach for High Impedance Fault detection in distribution system using Morphology Gradient filter. Journal of King Saud University - Engineering Sciences, 32(3), 177–185. https://doi.org/10.1016/j.jksues.2018.12.001

[13] Wang, B., Geng, J., & Dong, X. (2018). High-impedance fault detection based on nonlinear voltage–current characteristic profile identification. IEEE Transactions on Smart Grid, 9(4), 3783–3791. https://doi.org/10.1109/TSG.2016.2642988

[14] Vijayakumar, A., Alexander Stonier, A., Geno Peter, G., Kumaresan, P., & Reyes, E. M. (2022). A modified seven-level inverter with inverted sine wave carrier for pwm control. International Transactions on Electrical Energy Systems, 2022, e7403079. https://doi.org/10.1155/2022/7403079

[15] G. De Alvarenga Ferreira and T. Mariano Lessa Assis, 2019 IEEE PES Conf. Innov. Smart Grid Technol. ISGT Lat. Am. 2019 1 (2019).

[16] Aljohani, A., & Habiballah, I. (2020). High-impedance fault diagnosis: A review. Energies, 13(23), 6447. https://doi.org/10.3390/en13236447.

[17] Kar, S., & Samantaray, S. R. (2016). High impedance fault detection in microgrid using maximal overlapping discrete wavelet transform and decision tree. 2016 International Conference on Electrical Power and Energy Systems (ICEPES), 258–263. https://doi.org/10.1109/ICEPES.2016.7915940

[18] Geno Peter, A. A. Stonier, P. Gupta, D. Gavilanes, M. M. Vergara, and J. Lung sin, "Smart Fault Monitoring and Normalizing of a Power Distribution System Using IoT," Energies, vol. 15, no. 21, p. 8206, Jan. 2022, doi: 10.3390/en15218206.